Vertical drag force acting on intruders of different shapes in granular media

Author(s):
Zaidi, Ali A.; Müller, Christoph

Publication date:
2017

Permanent link:
https://doi.org/10.3929/ethz-b-000193133

Originally published in:
EPJ Web of Conferences 140, https://doi.org/10.1051/epjconf/201714002011

Vertical drag force acting on intruders of different shapes in granular media

Ali Abbas Zaidi[1], *Christoph* Müller[1,*]

[1]Laboratory of Energy Science and Engineering, Department of Mechanical and Process Engineering, ETH Zürich, 8092 Zürich, Switzerland

Abstract. The penetration of large objects into granular media is encountered commonly both in nature (e.g. impacts of meteors and projectiles) and engineering applications (e.g. insertion of tractor blades into sand). The motion of the impacting intruder in granular media is resisted by a granular drag force. In this work, we assess the effect of intruder shape on the granular drag force using discrete element modelling (DEM). The following intruder shapes were modelled: spherical, conical, cylindrical and cubical. We observed that the drag force can be described well by a power-law relationship with intrusion depth, independent of the intruder shape. However, the exponent of the power-law expression increases with increasing "flatness" of the intruder's impacting surface due to an increasing fraction of the granular media affected by the impact of the intruder.

1 Introduction

The insertion and impact of a solid object or intruder into a granular material is of both academic and industrial relevance. Typical examples include the formation of craters by the impact of meteors or projectiles, motion of wheels on gravel or sand , insertion of tractor blades or the penetration of a bullet into a bag of sand [1-5]. Previous work in this area has indicated that the granular drag force that acts on the intruder can be expressed as:

$$F(z,v) = F(z) + F(v) + F_0 \qquad (1)$$

where z is the intrusion depth and v is the velocity of the intruder [6-10]. In Eq. (1), F(z) is the depth dependent hydrostatic drag force, F(v) is the velocity-dependent viscous drag force and F_0 represents a friction-like force acting on the intruder [11]. In some work the frictional component of the drag force is included in the hydrostatic term [9]. Using experiments, Peng et al. [12] and Hill et al. [13] proposed a power law expression for F(z), viz. $F(z) = kz^c$. In this work, we focused on low speed intruder dynamics, hence F(v) is neglected (generally F(v) can be neglected for intruder velocities less than about 0.8 m/s).

So far, most reports concerning the drag force acting on an intruder in a granular media, have studied spherical intruders. There is very little information available on how intruder shape affects the drag force. Hence, this work assesses the effect of intruder shape on the hydrostatic component of the granular drag force, F(z), using discrete element model (DEM) simulations.

2 Formulations

The DEM implemented in this work uses a soft sphere model [14]. The inter-particle collisions are modelled by a combination of a linear spring, a dashpot and a friction slider. The normal, F_n, and tangential component, F_t, of the contact force are calculated according to:

$$\boldsymbol{F}_n = (-K_n\delta_n - \eta_n \boldsymbol{G}\cdot\boldsymbol{n})\boldsymbol{n} \qquad (2)$$

$$\boldsymbol{F}_t = -K_t\boldsymbol{\delta}_t - \eta_t\boldsymbol{G}_t \qquad (3)$$

$$\text{If } |\boldsymbol{F}_t| > f|\boldsymbol{F}_n| \qquad (4)$$

$$\boldsymbol{F}_t = -f|\boldsymbol{F}_n|\boldsymbol{t} \qquad (5)$$

where K is the spring constant, η is the damping coefficient, $\boldsymbol{G}$ is the vector describing the relative velocity between the interacting particles, $\mathbf{G_t}$ is the slip velocity of the contact point and f is the coefficient of friction. The subscripts n and t refer to the normal and tangential direction of the contact, respectively, and $\boldsymbol{n}$ and $\boldsymbol{t}$ are the unit vectors in the normal and tangential direction of the particle-particle contact, respectively. Contact detection for non-spherical intruders is performed by discretizing the surface of the intruder into small triangular elements. The normal and tangential force are calculated by determining the overlap between the particle and the triangular element as shown in Fig. 1. Once the overlap (δ), has been determined the contact forces are calculated according to Eqs (2-5)

* Corresponding author: muelchri@ethz.ch

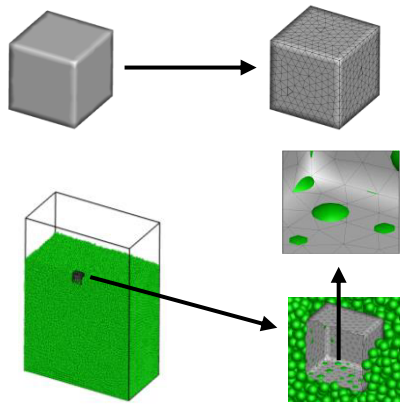

Fig. 1. Contact detection between the non-spherical intruder and particles.

The total force acing on an intruder is determined by summing up all forces acting on the elements of the intruder surface. Our numerical model was validated by MRI experiments and DEM simulations of spherical shaped intruders. In the latter validation case, a spherical intruder was pulled through a granular bed. The granular drag force calculated using the discretization scheme described above and using a conventional spherical DEM approach were compared. Good agreement between the different DEM schemes was observed.

3 Simulation Setup

To determine the drag force acting on non-spherical intruders in granular media, the following simulation set-up was used. The granular bed was contained in a rectangular container. The width, depth and height of the granular bed was 30×30×180 times the particle diameter (d_p). Particles were allowed to settle under gravity. The properties of particles used in the simulations are given in Table 1.

Table 1. Properties of the particles used.

d_p.	1.2 mm
Restitution coefficient	0.9
Friction coefficient	0.3
Elastic modulus	80000 N/m

The non-spherical intruders were pulled through the bed with a constant velocity of 0.2 m/s (hence, in a very good approximation, F(z) is the only component of the granular drag force that has to be considered). The shapes and sizes of the intruders simulated are summarized in Table 2. The small, medium and large sized intruders are referred to as, respectively, Case 1, Case 2 and Case 3 in the manuscript.

Table 2. Shapes and sizes of the intruder studied.

Intruder shape and direction of intrusion	Intruder dimensions
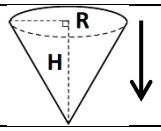	$H \times R = \begin{cases} 6d_p \times 3d_p \\ 12d_p \times 6d_p \\ 18d_p \times 9d_p \end{cases}$
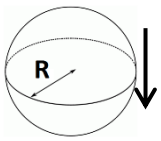	$R = 3d_p, 6d_p, 9d_p$
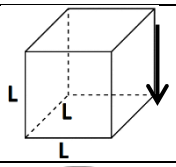	$L \times L \times L = \begin{cases} 6d_p \times 6d_p \times 6d_p \\ 12d_p \times 12d_p \times 12d_p \\ 18d_p \times 18d_p \times 18d_p \end{cases}$
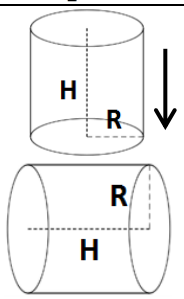	$H \times R = \begin{cases} 6d_p \times 3d_p \\ 12d_p \times 6d_p \\ 18d_p \times 9d_p \end{cases}$

In Table 2 the arrow indicates the direction of intrusion. For a cylindrical intruder two intrusion directions were studied.

4 Results & Discussions

Fig. 2 plots the granular drag force (divided by the intruder volume) as a function of the dimensionless intrusion depth (normalized by the height of the intruder) for different intruder shapes. The height of the granular bed was kept constant in all of the cases studied. We observe that independent of the intruder shape the drag force acting on the intruder follows a power law with intrusion depth *z*.

Similar to spherical intruders, dividing the drag force by the intruder volume leads to a size-independent power law expression for the drag force for all of particle shapes studied. We also observe that k $\approx 1.3 \times 10^{-4}$ independent of particle shape. However, the power-law coefficient c is a function of intruder shape and equals to 1.19, 1.3, 1.35, 1.38 and 1.41 for conical, spherical, cylindrical H, cylindrical V and cubic shapes, respectively (Table 3).

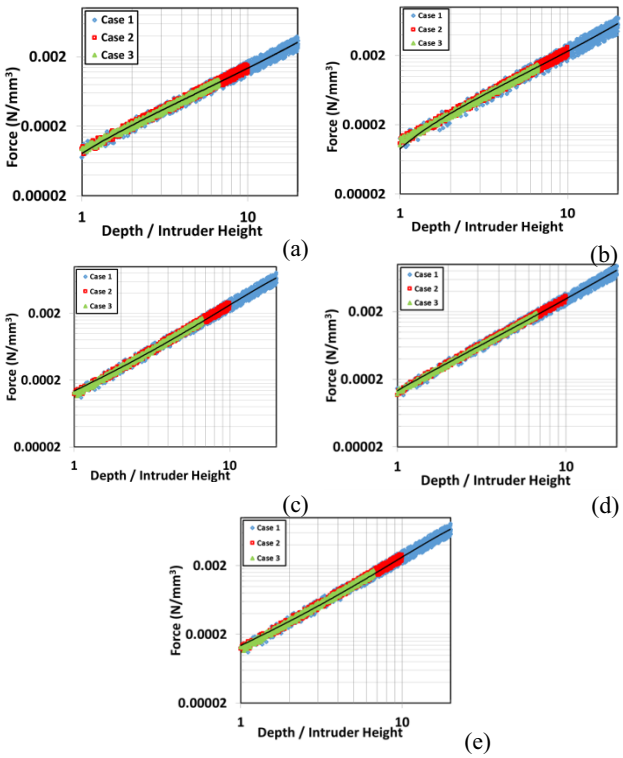

Fig. 2. Granular drag force acting on an intruder as a function of intrusion depth: (a) cone (b) sphere (c) cylinder configuration H (d) cylinder configuration V and (e) cube

Table 3. Expressions for the drag force for different intruder shapes.

Shape	**Power Law** $F(z) = kz^c$ $\left(k = 1.3 \times 10^{-4} \frac{\mathrm{N}}{\mathrm{mm}^{(c)}}\right)$
Cone	$F(z) = kz^{1.19}$
Sphere	$F(z) = kz^{1.3}$
Cylinder H	$F(z) = kz^{1.35}$
Cylinder V	$F(z) = kz^{1.38}$
Cube	$F(z) = kz^{1.41}$

It is worth noting that the value of c obtained for spheres is in agreement with previously reported experimental work [13]. Since for a given intrusion depth, cylinders and cubes experience a larger drag force than spheres or cones, it seems that the granular drag force increases with increasing "flatness" or "bluntness" of the impacting intruder surface.

To understand better this behaviour, we analysed in more detail the motion of particles around impacting intruders (Figs. 3 and 4). During the motion of the intruder, we determine the fraction of particles that have changed their original position (i.e. originally located in the purple box highlighted in Fig. 3).

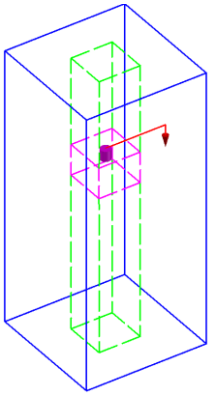

Fig. 3. Schematic diagram of a box that moves with the intruder and is used for data analysis. The dashed green lines highlight the path of the box during intruder motion

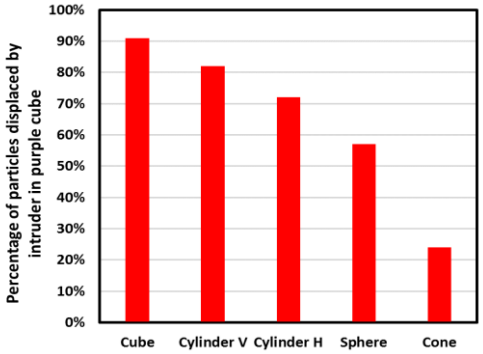

Fig. 4. Percentage of particles originally located in a box around the intruder that are affected by the motion of the intruder.

From Fig 4 we observe that the motion of a cubic intruder affects more particles than the motion of a conical intruder. The increase of the granular drag force (and the exponent of the power law) with an increase in intruder flatness hence, may be due to a higher energy loss due to a larger number of particle collisions.

5 Conclusions

The granular drag force acting on differently shaped intruders that are pulled with a constant velocity through a granular bed were studied using DEM. The following conclusions are drawn from this work:

(1) The hydrostatic component of the granular drag force obeys a power-law relationship with intrusion depth, independent of intruder shape.

(2) The granular drag force at a given intrusion depth increases with increasing"flatness" of the impacting intruder surface.

(3) The increasing exponent of the power-law relationship with increasing flatness of the intruder may be explained by an increasing number of particle-particle and particle-intruder collisions for "flatter" geometries.

Acknowledgement

The authors are grateful to the Swiss National Science Foundation (200021_153290) for financial support of this work.

References

1. R.A.F. Grieve, Nature **340**, 109 (1989)
2. H. Katsuragi, Lect. Notes Phys. **910**, 1 (2016)
3. A. H. Clark, L. Kondic, R.P. Behringer, Phys. Rev. Lett. **109**, 238302 (2012)
4. J. Crassous, D. Beladjine, A. Valance, Phys. Rev. Lett. **99**, 248001 (2007)
5. J. S. Uehara, M. A. Ambroso, R. P. Ojha, D. J. Durian, Phys. Rev. Lett **90**, 194301 (2003)
6. W. A. Allen, E. B. Mayfield, H. L. Morrison, J. Appl. Phys. **28**, 370 (1957)
7. M. J. Forrestal, V. K. Luk, Int. J. Impact Eng. **12**, 427 (1992)
8. D. I. Goldman, P. Umbanhowar, Phys. Rev. E **77**, 020101 (2008)
9. H. Katsuragi, D. J. Durian, Nat. Phys. **3**, 420 (2007)
10. P. Umbandowar, D. I. Goldman, Phys. Rev. E **82**, 010301 (2010)
11. M. Hou, Z. Peng, R. Liu, Y. Wu, Y. Tian, K. Lu, C. K. Chan, Sci. Technology Adv. Mat. **6**, 855 (2005)
12. Z. Peng, X. T. Xu, K. Q. Lu, M. Y. Hou, Phys. Rev. E **80**, 020101(R) (2009)
13. G. Hill, S, Yeung, S, A, Koehler, Europhys. Lett. **72**, 137 (2005)
14. P. A. Cundall, O. D. L. Strack, Geotechnique **29**, 47 (1979)